Post-Compensation of Nonlinear Distortions of 64-QAM Signals in a Semiconductor Based Wavelength Converter

Benoît Filion, An T. Nguyen, Leslie A. Rusch, and Sophie LaRochelle

Journal of Lightwave Technology, (Volume 33, Issue 15) (2015)

Doi: 10.1109/JLT.2015.2436812

http://ieeexplore.ieee.org/document/7112081/?arnumber=7112081

Post-Compensation of Nonlinear Distortions of 64-QAM Signals in a Semiconductor Based Wavelength Converter

Benoît Filion, *Graduate Student Member, IEEE*, An T. Nguyen, *Graduate Student Member, IEEE*, Leslie A. Rusch, *Fellow, IEEE*, and Sophie LaRochelle, *Fellow, OSA, Senior Member, IEEE*

***Abstract*—** We experimentally investigate post-compensation of nonlinear distortions induced by a wavelength converter (WC) based on four-wave mixing in a semiconductor optical amplifier. The technique exploits a low-complexity digital filter-based back-propagation (DFBP) method. We perform post-compensation of nonlinear distortions following single stage wavelength conversion of 5 Gbaud 64- quadrature amplitude modulation (QAM). We examine the DFBP performances in the presence of a degraded optical signal-to-noise ratio at the WC input and we explore the WC optimal operating conditions. Also, we experimentally demonstrate for the first time in the literature dual stage wavelength conversion of QAM signals, in particular, 5 Gbaud 64-QAM, and show that bit error rate below hard-decision forward error correction threshold is only possible with post-compensation of nonlinear distortions. These results are of importance for the development of wavelength routed networks requiring successive wavelength conversion stages to enhance routing capabilities.

***Index Terms*—Advanced modulation formats, coherent detection, four-wave mixing, optical wavelength conversion, quadrature amplitude modulation, semiconductor optical amplifiers.**

I. Introduction

Wavelength converters (WCs) are essential building blocks enabling future all-optical wavelength routed networks with sub-wavelength granularity switching such as optical burst switching (OBS) and optical packet switching (OPS). In these networks, the wavelength dimension is used not only for routing, but also for contention resolution, i.e., when two input signals sharing the same wavelength are destined to the same optical fiber. Wavelength-based contention resolution is the most effective technique as it does not incur additional latency while maintaining the shortest path or minimum hop distance [1]. Furthermore, OBS and OPS technology have also been proposed for data centers [2], [3].

Coherent systems using advanced modulation formats together with digital signal processing have recently been adopted in optical communication systems to provide increased spectral efficiency. While coherent detection is already established as the technology of choice in long haul communication systems, as component cost decline this technology is expected to enter metropolitan area networks and access networks. Due to the shorter reach of such networks, the use of highly spectrally efficient advanced modulation formats such as M-ary quadrature amplitude modulation (QAM), from 16-QAM up to 64-QAM, will greatly enhance their capacity [4]. Coherent systems further enables flexible and agile transparent networks that adapt parameters such as data rate, frequency spacing and modulation format according to desired reach and volume of traffic [4]–[7]. In this context, thorough investigation and optimization of wavelength converters for advanced modulation formats is needed in order to enable future all-optical wavelength routed networks.

Four-wave mixing (FWM) in semiconductor optical amplifiers (SOAs) is an efficient and practical wavelength conversion mechanism because of its compactness, low pump powers, high conversion efficiency (CE) and transparency to modulation formats [8]. Regarding phase-modulated formats, we showed in [9] that a careful optimization of the signal and pump power is required to tradeoff the benefits of a high conversion efficiency and the penalties created by induced nonlinearities during the FWM process. Using two-pumps, wavelength conversion covering the whole C-band is possible as demonstrated in [9].

In reference [10], we 1) introduced for the first time the digital filter-based back-propagation (DFBP) method for the compensation of nonlinear distortions introduced by SOA WCs of phase (QAM) modulated signals; 2) investigated the approach through numerical simulations and verified, through these calculations, the required sampling rate to implement the filter; and 3) validated all the results through experimental measurements. The experimental measurements were done in a very simple single stage scenario and with ideal optical signal-to-noise ratio (OSNR) at the input of the WC (>35 dB). The only parameter that was swept was the input signal power.

In this paper, we address the issue of compensation of nonlinear distortions of 64-QAM signals when the input OSNR is degraded, for example by amplified spontaneous emission (ASE) accumulated during successive optical amplifications or wavelength conversion. This is an important issue for future applications in wavelength routed networks cascading several wavelength conversion stages. The main contribution of this paper is to investigate how DFBP techniques can improve the performance of the WC in the presence of a noisy signal and to

This work was supported by Natural Sciences and Engineering Research Council (NSERC) of Canada and by the Canada Research Chair APTECS.

The authors are with the Department of Electrical and Computer Engineering and the Center for Optics, Photonics and Lasers (COPL), Université Laval, Pavillon d'Optique-Photonique, 2375 de la Terrasse, Québec (QC) G1V 0A6, Canada (e-mail: sophie.larochelle@gel.ulaval.ca).

determine its optimal operating conditions. More specifically, we 1) experimentally demonstrate performance improvement that can be achieved by using DFBP when the input OSNR is degraded to 25 dB; 2) sweep both signal power and received OSNR experimentally to identify the optimal operating conditions of the SOA WC; 3) show that DFBP can allow the pump power to be reduced from 10 dBm to 5 dBm without bit error rate (BER) penalty; and 4) perform for the first time to our knowledge two successive wavelength conversions on a 64-QAM signal; and 5) show how DFBP can help to improve the robustness of the cascaded system, for example with respect to variations in signal power and link loss.

This paper is organized as follows. In section II, we briefly present the equations required to implement DFBP. In section III, we describe the experimental setups. We present the experimental results of 5 Gbaud 64-QAM single stage wavelength conversion in section IV and the experimental results of dual stage wavelength conversion follow in section V.

II. Digital Filter-Based Back-Propagation

FWM in a SOA is achieved by simultaneously injecting at its input one continuous wave (CW) signal, called the pump, together with the data modulated signal to be converted. The gain and the refractive index of the amplifier are then modulated at the frequency detuning Ω, defined as the optical frequency separation between the signal and the pump [8]. A new optical field, the conjugate, is generated during the propagation within the SOA.

The post-compensation technique is based on a small-signal analysis of the SOA dynamic rate equation governing nearly degenerate FWM, in which only the carrier density modulation is considered. In this section, we introduce the necessary equations and discuss the physical parameters needed for the DFBP implementation (the complete analysis can be found in [10]).

The optical field at the input of the SOA, E_{in}, consists of a pump E_p centered at ω_p, and a modulated, weaker signal E_s centered at ω_s leading to

$$E_{in}(t) = E_p + E_s(t)e^{j\Omega t}, \quad \Omega = \omega_p - \omega_s. \tag{1}$$

Under small-signal analysis [11], the equation for the conjugate field E_c at the SOA output is given by

$$E_c(t) = e^{h(t)\frac{(1-j\alpha)}{2}} F(t,\Omega) E_p^2 E_s^*(t) \tag{2}$$

where

$$F(t,\Omega) = -\frac{(1-j\alpha)}{2P_{sat}} \frac{\left(e^{h(t)}-1\right)}{\left(1+e^{h(t)}\frac{|E_p|^2+|E_s(t)|^2}{P_{sat}} - j\Omega\tau_s\right)}. \tag{3}$$

In (2) and (3), $h(t)$ is the integrated gain, α is the linewidth enhancement factor, τ_s is the carrier lifetime and P_{sat} is the saturation power. We note that $h(t)$ represents the baseband part of the integrated gain, including sidebands located at the frequency detuning Ω. The rate equation governing the dynamics of $h(t)$ is given by

$$\frac{\partial h(t)}{\partial t} = \frac{h_0 - h(t)}{\tau_s} - \left(e^{h(t)}-1\right)\frac{\left(|E_p|^2+|E_s(t)|^2\right)}{\tau_s P_{sat}}. \tag{4}$$

where h_0 is the small-signal integrated gain. As seen in (2), the temporal variation of $h(t)$ induces nonlinear distortions on the conjugate $E_c(t)$. To solve (4) for a given input power, we write the gain as its mean value plus a zero-average perturbation term, i.e., $h(t) = \bar{h} + \delta h(t)$. Since the instantaneous input signal power $|E_s(t)|^2$ is unknown at the receiver, we find an estimate $|\hat{E}_s(t)|^2$ with the knowledge of $E_c(t)$ at the receiver and (2) leading to

$$|\hat{E}_s(t)|^2 = \frac{|E_c(t)|^2}{e^{h(t)} \times |F(\Omega)|^2 \times |E_p^{\,2}|^2}. \tag{5}$$

Under the small-signal approximation ($\delta h(t) \ll \bar{h}$) and replacing $|E_s(t)|^2$ by $|\hat{E}_s(t)|^2$ in (4), we find that the SOA acts as a low-pass filter according to

$$\delta h(t) = K \cdot m(t) \otimes \delta p_c(t) \tag{6}$$

where K is given by

$$K = -\frac{e^{\bar{h}}-1}{1+e^{\bar{h}}\bar{p}_p + e^{-\bar{h}}\bar{p}_c}, \tag{7}$$

$\bar{p}_p$ and $\bar{p}_c$ are the average pump and conjugate power defined in (9) below, while $m(t)$ is a single-pole low-pass filter with time constant

$$\tau_{eff} = \frac{\tau_s}{1+e^{\bar{h}}\bar{p}_p + e^{-\bar{h}}\bar{p}_c}. \tag{8}$$

In (6)-(8), we normalized the input powers by the SOA saturation power, P_{sat}. We apply the same definition for the average component and time varying parts, noting that the pump has constant power we write $|E_p|^2/P_{sat} = \bar{p}_p$ and for the conjugate

$$p_c(t) = \bar{p}_c + \delta p_c(t) = \frac{|E_c(t)|^2}{P_{sat} \times |F(\Omega)|^2 \times |E_p^{\,2}|^2}. \tag{9}$$

Taking the Laplace transform of $K \cdot m(t)$ and applying the bilinear transform [12] leads to the following discrete impulse response of the digital filter

$$\delta h[n] = B\delta h[n-1] + C\delta p_c[n] + C\delta p_c[n-1] \tag{10}$$

where $x[n] \cong x(n\Delta t)$ for any continuous waveform $x(t)$, Δt is the sampling time,

$$B = \frac{1 - 2\tau_{eff}/\Delta t}{1 + 2\tau_{eff}/\Delta t}, \tag{11}$$

and

$$C = \frac{K}{1 + 2\tau_{eff}/\Delta t}. \tag{12}$$

Finally, the post compensated conjugate $\hat{E}_c(t)$ is obtained with

$$\hat{E}_c(t) = E_c(t) e^{\frac{-(1+j\alpha)}{2} \times (\bar{h} + \delta h(t))}. \tag{13}$$

With the knowledge of $E_c(t)$ at the receiver, a digital filter (equations (10) to (12)) can be implemented to post-compensate the conjugate. Further details on the implementation including the block diagram of the algorithm can be found in [10]. As described in Appendix A, the use of this post-compensation technique requires the characterization of only a few standard SOA parameters including α, P_{sat}, τ_s and the small signal gain $G_0 = exp(h_0)$.

III. Experimental Setup

The experimental setup is presented in Fig. 1(a). A tunable laser at λ_s = 1549.3 nm (1548.4 nm for the dual-stage wavelength conversion experiments) is modulated by an in-phase/quadrature Mach-Zehnder modulator (IQ-MZM). The IQ-MZM is driven by a digital to analog converter (DAC) with 3 bits resolution that is in turn driven by 3-level data streams of $2^7 - 1$, $2^{11} - 1$ and $2^{20} - 1$ pseudo-random-bit-sequences. A phase shifter is used to decorrelate the data streams in order to generate the in-phase and quadrature components. The modulator output is fed into a variable optical attenuator (VOA1) and a erbium-doped fiber amplifier (EDFA1) followed by a Gaussian shaped optical filter (OF1) with 1 nm bandwidth tuned at λ_s, a polarization controller (PC), a VOA (VOA2) and then into the WC. The signal OSNR, measured over a bandwidth of 0.1 nm, is adjusted by varying the attenuation (VOA1) and the gain of the EDFA (EDFA1).

After wavelength conversion, the FWM term, i.e., the conjugate, goes directly to the pre-amplifier. The conjugate power at the input of the coherent receiver (CRx) is kept fixed at -6 dBm for all wavelength conversion experiments and coherently detected using a tunable laser at λ_{lo} as local oscillator (LO). The noise loading stage is composed of an EDFA (EDFA3) followed by an OF (OF3), with identical shape (Gaussian) and bandwidth (0.7 nm) as the pre-amplified receiver OF (OF2), and a VOA (VOA3). The filtered ASE noise coming from the EDFA (EDFA3) is combined with the conjugate with a 2×1 coupler. The OSNR at the input of the pre-amplified receiver is set by adjusting the VOA (VOA3) of the noise loading stage while the conjugate power remains

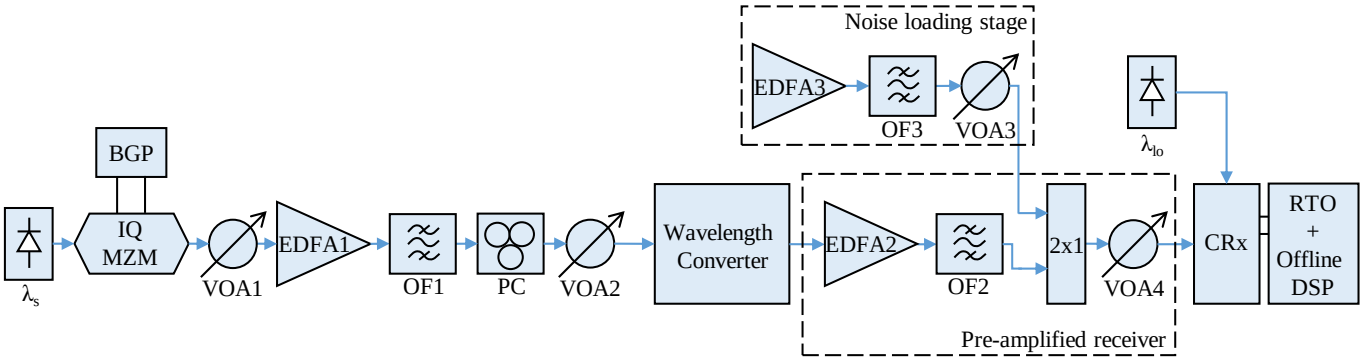

(a)

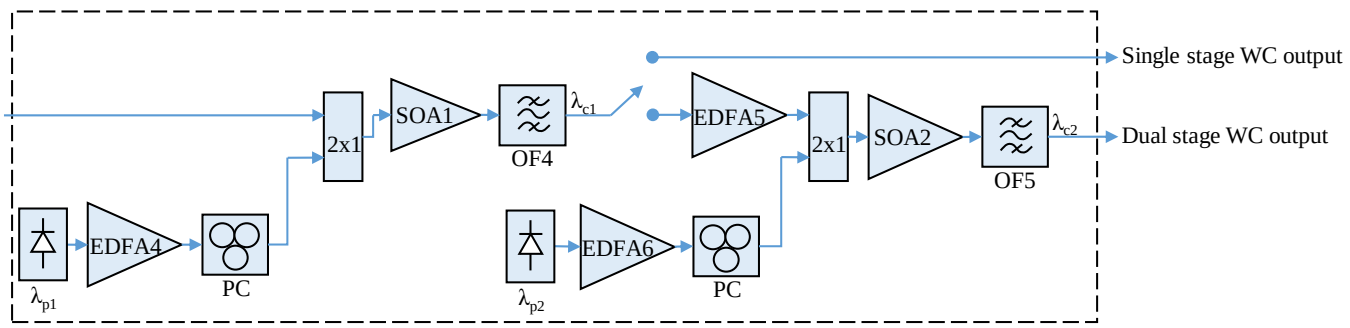

(b)

Fig. 1 Block diagram of a) the experimental setup and b) the wavelength converter.

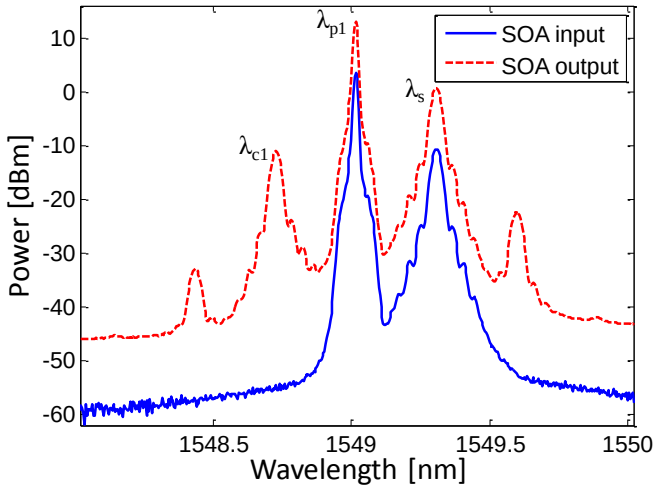

Fig. 2 Typical optical spectra at the input (solid line) and at the output (dashed line) of a single stage wavelength conversion.

following phase recovery. Finally, hard-threshold decision is performed on I and Q individually, we count the errors and estimate BER.

The block diagrams of the WC is shown Fig. 1(b). A tunable laser delivering the pump at $\lambda_{p1} = 1549$ nm (1548.1 nm for the dual-stage wavelength conversion experiments[1]) is amplified by an EDFA (EDFA4) and followed by a PC. The signal and the pump are combined using a 2×1 coupler injected into a nonlinear SOA (SOA1) (SOA1117/CIP) operating over the C-band (1528 nm to 1562 nm) with 20 dB small-signal gain, 9 dBm output saturation power and < 1 dB polarization dependent gain. Two isolators (not shown in Fig. 1(b) are used before and after the SOA to suppress back reflections. The conjugate at λ_{c1} is filtered with a programmable OF (OF4) (WaveShaper 1000S/Finisar). The optical filter (OF4) is Gaussian shaped and its bandwidth carefully chosen to obtain the best compromise between pump power suppression and conjugate power transmission. For the dual stage wavelength conversion experiments, the conjugate at $\lambda_{c1} = 1548.7$ nm (1547.8 nm for the dual-stage wavelength conversion experiments) is amplified by an EDFA (EDFA5) in order to compensate for the

at the input (solid line) and at the output (dashed line): a) of the first wavelength conversion stage and b) of the second wavelength

are all duplicates of the first WC stage. The wavelength detuning is $\Omega = 0.3$ nm for both the first WC stage ($\lambda_s - \lambda_{p1}$) and the second WC stage ($\lambda_{c1} - \lambda_{p2}$).

Typical spectrums for the SOA input and output of single stage wavelength conversion experiments are shown in Fig. 2. For the dual stage wavelength conversion experiments, typical spectrums of the SOA input and output of the first and second wavelength conversation stage are shown in Fig. 3(a) and Fig. 3(b) respectively. The optical spectra were measured with an optical spectrum analyzer with 0.01 nm resolution. The discrepancy of the noise floor in Fig. 3, compared to Fig. 2, is caused by the optical couplers (not shown in Fig. 1) that were used for signal monitoring: because of the additional loss, the

[1] Because the single pump experiments and the dual pump experiments were not done at the same time, slightly different signal wavelengths were used for each experiments. This wavelength difference (0.9 nm) is small compared to the SOA bandwidth and has no impact on the WC and DFPB performance.

ASE noise lies under the noise floor of the optical spectrum analyzer. Considering the relatively low baud rate (5 Gbaud) and the wavelength spacing (0.3 nm) used in our experiments, the impact of CE non-uniformity is negligible.

IV. Single Stage Wavelength Conversion

A. *DFBP robustness against ASE noise*

We compare the measured error vector magnitude (EVM) and BER as a function of the OSNR at the receiver for different operating conditions, i.e., input pump and signal power, before and after DFBP. In order to investigate the robustness of the DFBP technique against ASE noise, we also measured the EVM and BER for a degraded OSNR at the input of the WC. Note that the EVM is displayed in the form of differential EVM, ΔEVM, defined as the difference between the measured EVM before and after post-compensation using DFBP. As for the BER measurements, separate BER curves are shown before and after DFBP.

Measurements in Fig. 4 were done with an input OSNR of 35 dB. The pump power was either 5 dBm or 10 dBm and the input signal power varied between -2 dBm to -12 dBm. The received OSNR was swept between 18 dB to 28 dB. Note that for the reminder of the paper the term OSNR will refer to the OSNR at the coherent receiver, while $OSRN_{in}$ represents the OSNR at the input of the SOA. As previously demonstrated in [10], more nonlinearities are induced on the conjugate during the FWM process as the injected pump power decreases and/or the input signal increases. Thus, we expect the EVM improvement due to the application of the DFBP technique to be more significant in such conditions. By comparing Fig. 4(a) ($P_p = 5$ dBm) to Fig. 4(b) ($P_p = 10$ dBm), we effectively observe this behavior: for the same input signal power value, ΔEVM is always higher with $P_p = 5$ dBm compared to $P_p = 10$ dBm. Additionally, for either ΔEVM plot (Fig. 4(a) or Fig. 4(b)), we see the best ΔEVM for the strongest signals, and worst ΔEVM for the weakest signals. We note that ΔEVM tends to slightly degrade for lower OSNR as the conjugate becomes more limited by the ASE noise. For instance, for $P_p = 5$ dBm and $P_s = -2$ dBm, ΔEVM= 2.7% with 28 dB OSNR while ΔEVM= 1.3% with 18 dB OSNR (see Fig. 4(a)).

BER measurements are presented Fig. 4(c) and Fig. 4(d) for a pump power of 5 dBm and 10 dBm, respectively. Solid lines represent BER before DFBP, while dashed lines show improved BER after DFBP. BER results are presented only for input signal powers where BER fell below the hard decision forward error correction (FEC) threshold of 2×10-3 [16] (either before or after DFBP). After post-compensation, the BER is

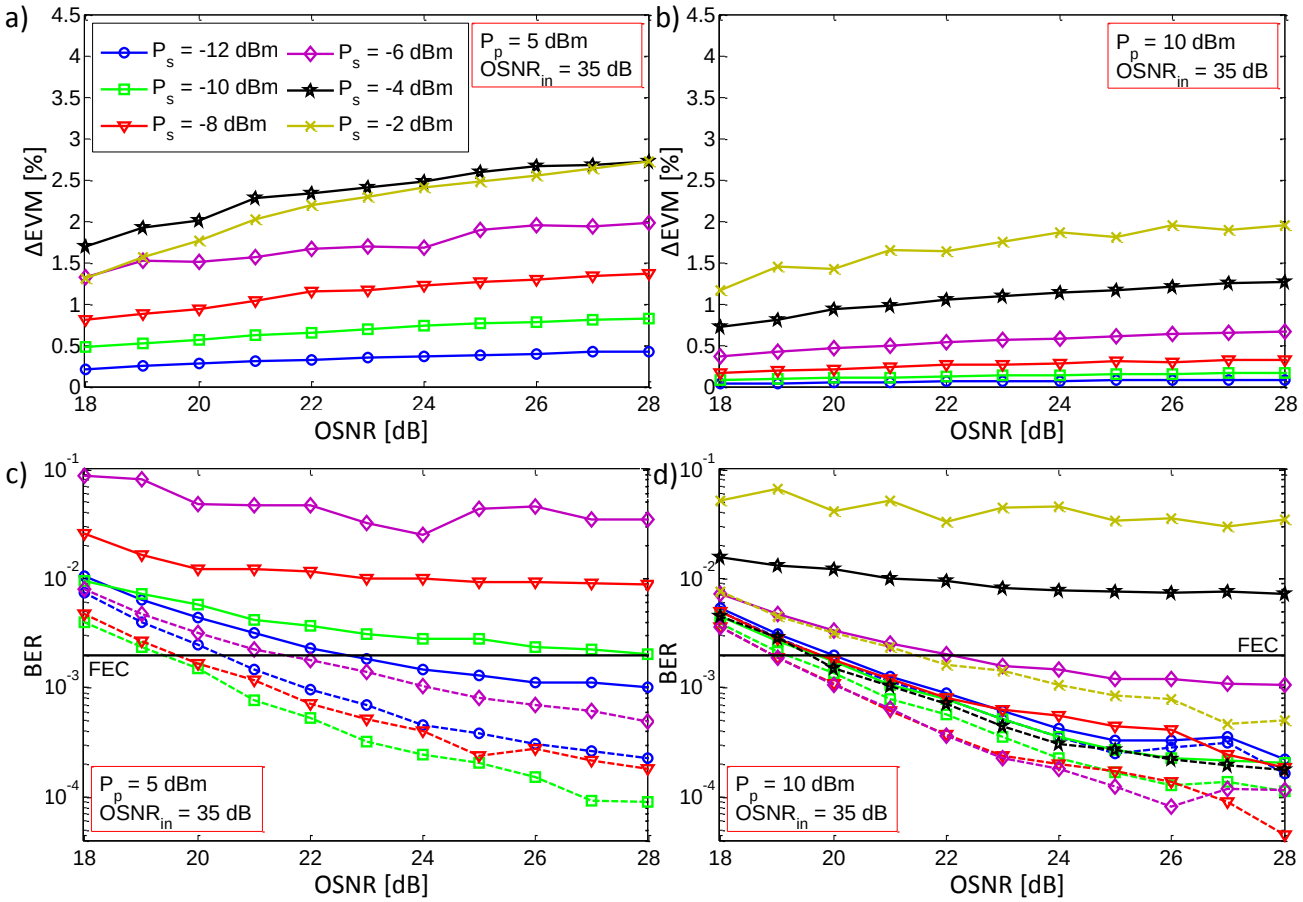

Fig. 4 Measured differential EVM (ΔEVM) and BER, before DFBP (solid lines) and after DFBP (dashed lines), as a function of the received OSNR of 5 Gbaud 64-QAM single stage wavelength conversion for an input OSNR of 35dB with received constellations examples: a) ΔEVM for a pump power of 5 dBm b) ΔEVM for a pump power of 5 dBm c) BER for a pump power of 5 dBm and d) BER for a pump power of 10 dBm.

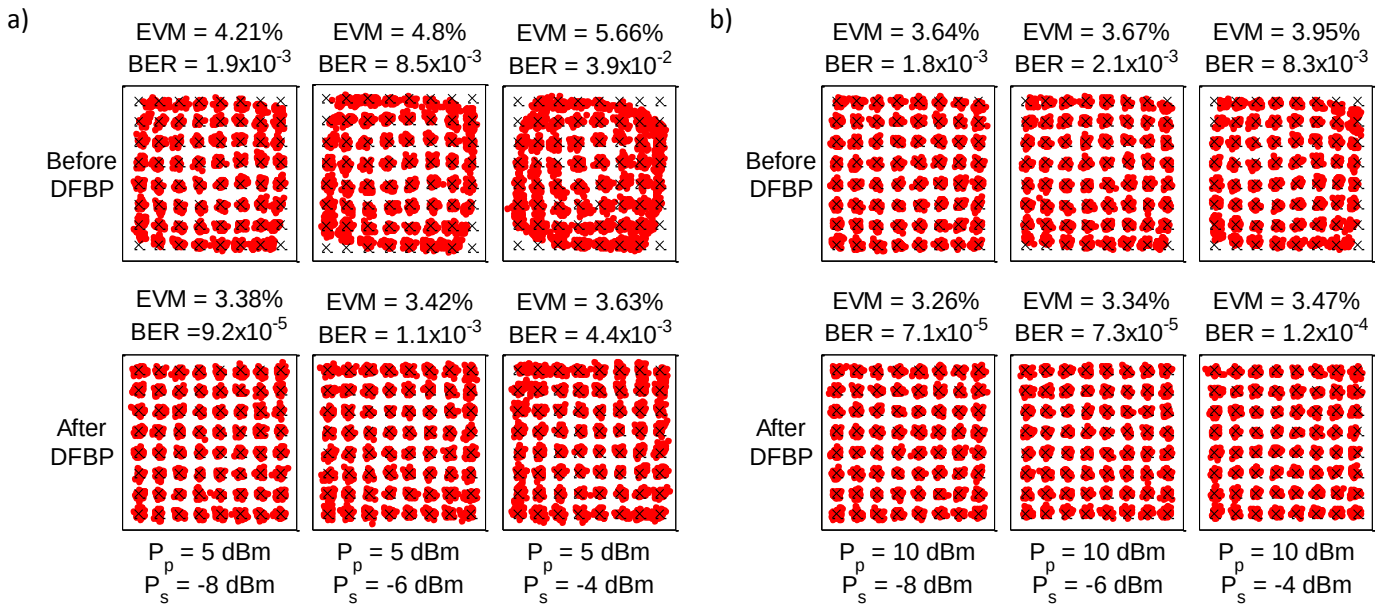

Fig. 5 Constellation examples before DFBP and after DFBP of 5 Gbaud 64-QAM single stage wavelength conversion for an input OSNR of 35dB: a) for a pump power of 5 dBm and b) for a pump power of 10 dBm.

optimal signal power is -12 dBm before DFBP and -10 dBm after DFBP. This is caused by the tradeoff between the nonlinearities and ASE noise at the receiver and is discussed in details in the next section. By comparing the best case before DFBP (P_s = -12 dBm) and after DFBP (P_s = -10 dBm), the OSNR improvement at the FEC threshold after DFBP is ~3.2 dB. With P_p = 10 dBm (Fig. 4(d)), BER below the FEC is obtained with a signal power up to -6 dBm before DFBP and up to -2 dBm after DFBP. Before DFBP, the best performance is obtained with P_s = -10 dBm and with P_s = -6 dBm / P_s = -8 dBm after DFBP, with an OSNR improvement at the FEC threshold of ~0.8 dB. We note that, before DFBP, there is ~2.2 dB in OSNR penalty with P_s = -6 dBm compared to P_s = -8 dBm while they exhibit the same performance after DFBP, meaning that the additional nonlinearities with the higher signal power have been compensated. As with the EVM measurements, at either pump power we observe slightly degraded DFBP performance for lower OSNR. Examples of received constellations before and after DFBP are shown for P_p = 5 dBm and P_p = 10 dBm in Fig. 5(a) and Fig. 5(b) respectively.

The experimental results with a degraded input OSNR of 25 dB are shown in Fig. 6: ΔEVM for a pump power of 5 dBm (Fig. 6(a)) and 10 dBm (Fig. 6(b)), BER before (solid lines) and after (dashed lines) DFBP for a pump power of 5 dBm (Fig. 6(c)) and 10 dBm (Fig. 6(d)). These results confirm that the DFBP post-compensation technique still provide performance improvement in the presence of a noisy signal at the WC input. threshold is obtained only for P_s = -12 dBm before DFBP and up to P_s = -6 dBm after DFBP. In that context, the optimal signal power is the same before and after DFBP, i.e., P_s = -12 dBm, with ~1.8 dB OSNR improvement after DFBP. In Fig. 6(d), with P_p = 10 dBm, BER below the FEC threshold is obtained up to P_s = -6 dBm before DFBP and up to P_s = -2 dBm after DFBP. ~0.8 dB OSNR improvement is obtained after DFBP (P_s = -8 dBm) at the FEC threshold compared to before DFBP (P_s = -10 dBm). Examples of received constellations before and after DFBP are shown for P_p = 5 dBm and P_p = 10 dBm in Fig. 7(a) and Fig. 7(b) respectively.

B. WC optimal operating condition

We investigate the optimal operating conditions of the WC, i.e., input pump and signal power. For advanced modulation formats, we found that the optimal operating conditions depend on the amount of loss between the WC and the receiver. Indeed, the OSNR at the CRx depends on the conjugate power since the EDFA gain at the pre-amplifier input (EDFA2 in Fig. 1(a)) is adjusted to keep a fixed power at the CRx. However, in [17], we showed that there is a tradeoff between the received OSNR and the nonlinear distortions. Optimizing the pump power for maximum CE, defined as the ratio of conjugate power to the input signal power, does not translate into an optimal EVM: better CE exhibits higher OSNR at the CRx, as less gain is needed at the pre-amplified receiver, but also leads to more nonlinear distortions induced during the wavelength conversion process. Note that our optimization here is limited to two input pump power values, i.e., 5 dBm and 10 dBm. These values were chosen in order to investigate the tradeoff between the received

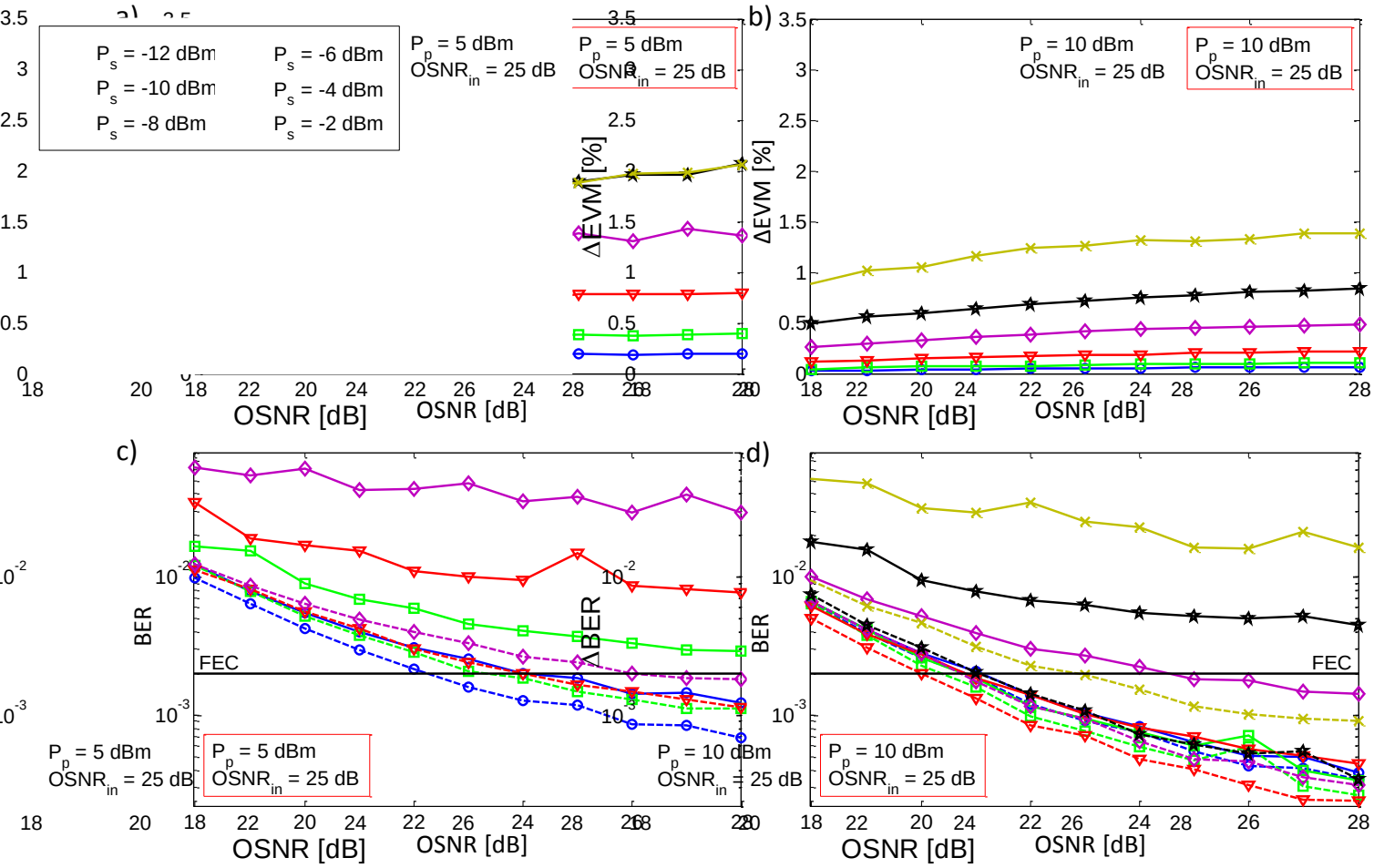

Fig. 6 Measured differential EVM (ΔEVM) and BER, before DFBP (solid lines) and after DFBP (dashed lines), as a function of the received OSNR of 5 Gbaud 64-QAM single stage wavelength conversion for an input OSNR of 25dB with received constellations examples: a) ΔEVM for a pump power of 5 dBm b) ΔEVM for a pump power of 5 dBm c) BER for a pump power of 5 dBm and d) BER for a pump power of 10 dBm.

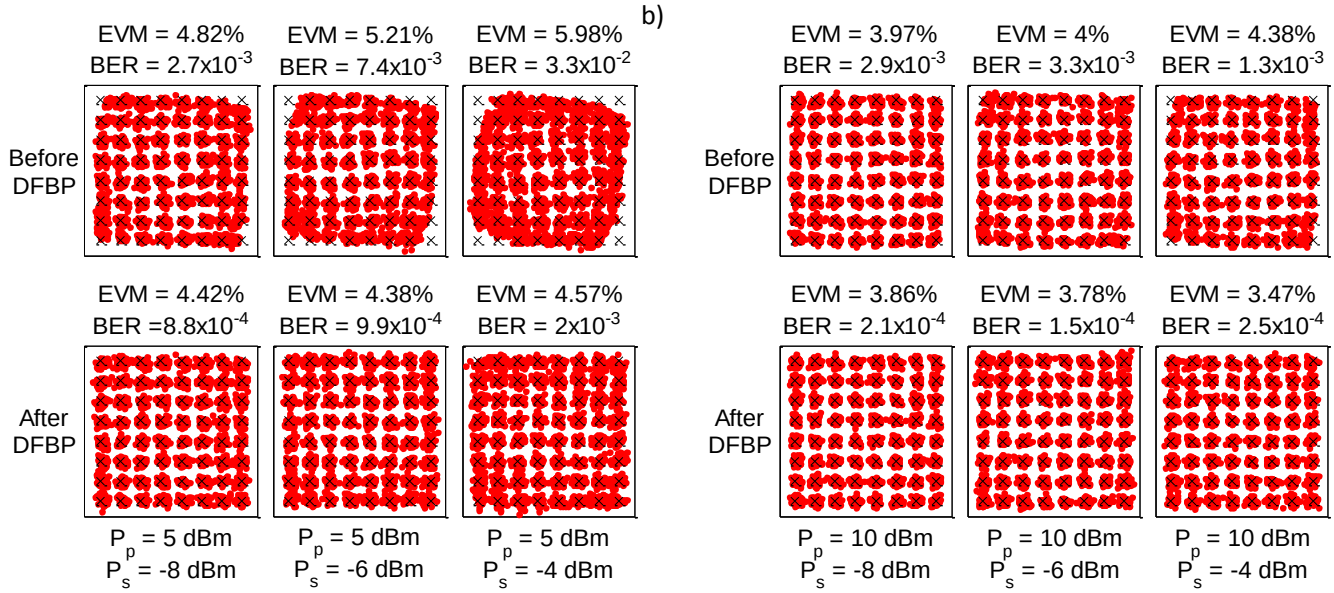

Fig. 7 Constellation examples before DFBP and after DFBP of 5 Gbaud 64-QAM single stage wavelength conversion for an input OSNR of 25dB: a) for a pump power of 5 dBm and b) for a pump power of 10 dBm.

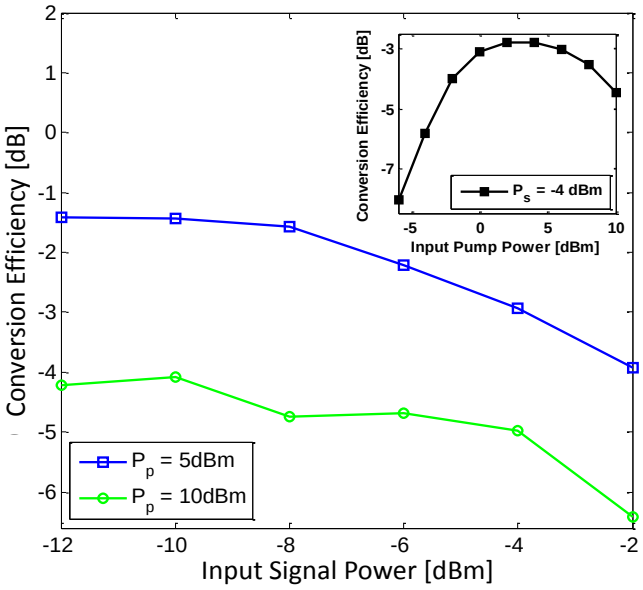

Fig. 8 Measured conversion efficiency of 5 Gbaud 64-QAM single stage wavelength conversion with 35 dB input OSNR. The inset shows the conversion efficiency as a function of the input pump power for an input signal power of -4 dBm.

OSNR and the nonlinear distortions, as shown later in this section. Although for this purpose these two pump power values were sufficient, a full WC operating condition optimization would require a complete sweep of pump power values. The measured CE as a function of the WC operating conditions, with an input OSNR of 35 dB, is shown in Fig. 8: the inset shows an example of CE measurements as a function of the input pump power for an input signal power of -4 dBm. Injecting more signal power at the WC input, to obtain better OSNR at the CRx, also comes with a cost of increased conjugate nonlinearities. Finally, the loss following the WC, which may come from either insertion loss from optical components or simply propagation loss, will further limit the received OSNR. Consequently, optimizing the WC operating condition must take into account the link loss that will impact the tradeoff between OSNR and nonlinearities.

As discussed in section II, we measured the EVM and BER as a function of the OSNR while keeping the conjugate power

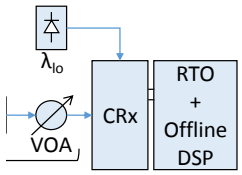

eceiver

ıd BER measurements as a
ı conversion.

ınique (see Fig. 1(a)).
predict the EVM and
WC. We use a well-
18], to calculate the
ık displayed in Fig. 9.
ansform the received

the optimal operating
ı the measured EVM
link loss of 0 dB (Fig.
(Fig. 10(c)). Without DFBP, when using a low pump power $P_p = 5$ dBm, the converted signal EVM at the coherent receiver is mostly limited by the nonlinearities. Thus, a low optimal signal power at the WC input ($P_s = -10$ dBm in Fig. 10(a), Fig. 10(b) and Fig. 10(c)) is the optimal choice as it minimizes the nonlinearities induced inside the WC. However, after DFBP, the ideal tradeoff between OSNR and nonlinearities changes and the optimal signal power at the WC input tends to shift towards increasing values. In other words, using the post-compensation technique, we can inject more signal power at the WC input and thus obtain better OSNR at the coherent receiver without the additional penalty coming from the nonlinearities. For instance, the optimal signal power becomes $P_s = -6$ dBm with $P_p = 5$ dBm for a 14 dB link loss as seen in Fig. 10(c). Because of the reduced CE with a higher pump power $P_p = 10$ dBm, the change of the optimal WC operating condition after DFBP is already observed for a minimal link loss (0 dB) as it shifts from $P_s = -10$ dBm to $P_s = -6$ dBm (see Fig. 10(a)). Furthermore, the EVM worsen when the input signal power is below $P_s = -10$ dBm, also for the same reason.

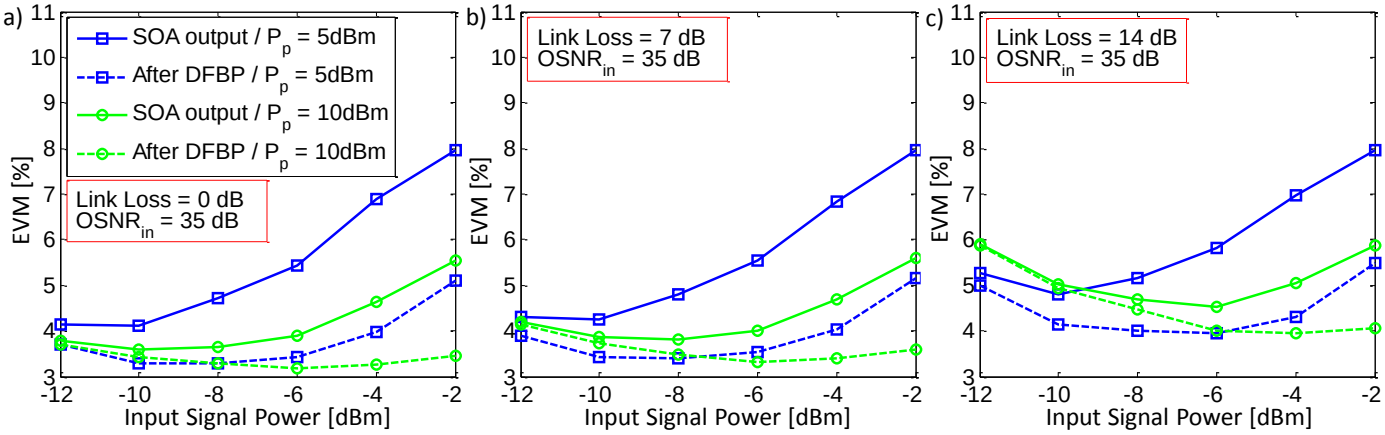

Fig. 10 Measured EVM as a function of the input signal power of 5 Gbaud 64-QAM single stage wavelength conversion with 35 dB input OSNR for a link loss of a) 0 dB b) 7 dB and c) 14 dB. The EVM is shown before and after application of the DFBP post-compensation technique.

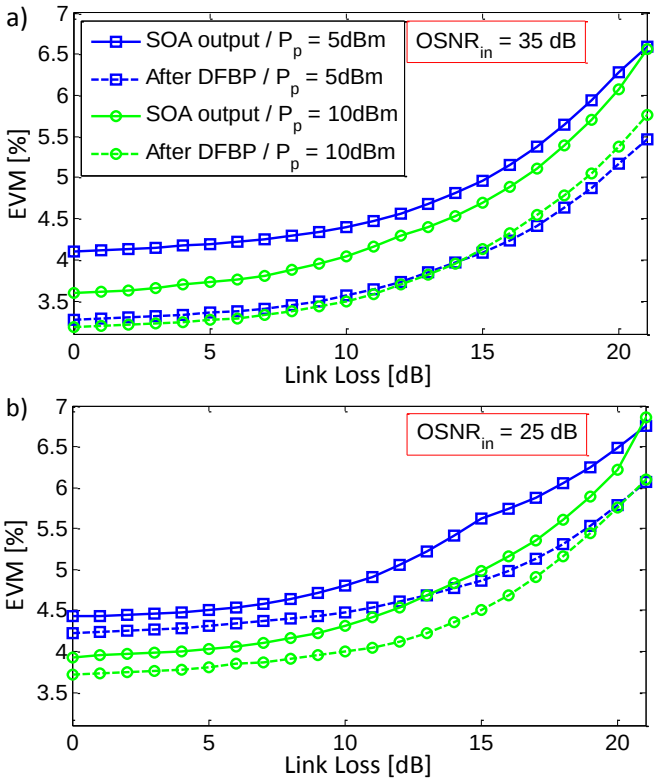

Fig. 11 Measured EVM with an optimal input signal power as a function of the link loss of 5 Gbaud 64QAM single stage wavelength conversion before and after application of the DFBP post-compensation technique with (a) 35 dB input OSNR and (b) 25 dB input OSNR.

Fig. 11 shows the optimal EVM, i.e. with the optimal signal power for a pump power $P_p = 5$ dBm and $P_p = 10$ dBm, as a function of the link loss with 35 dB input OSNR and 25 dB input OSNR. The optimal input signal power $P_s = -6$ dBm. Furthermore, assuming a standard hard-decision forward error correction threshold (FEC) of 2×10^{-3}, we obtain as much as 2.9 dB link loss gain after DFBP. Significant BER improvement is also

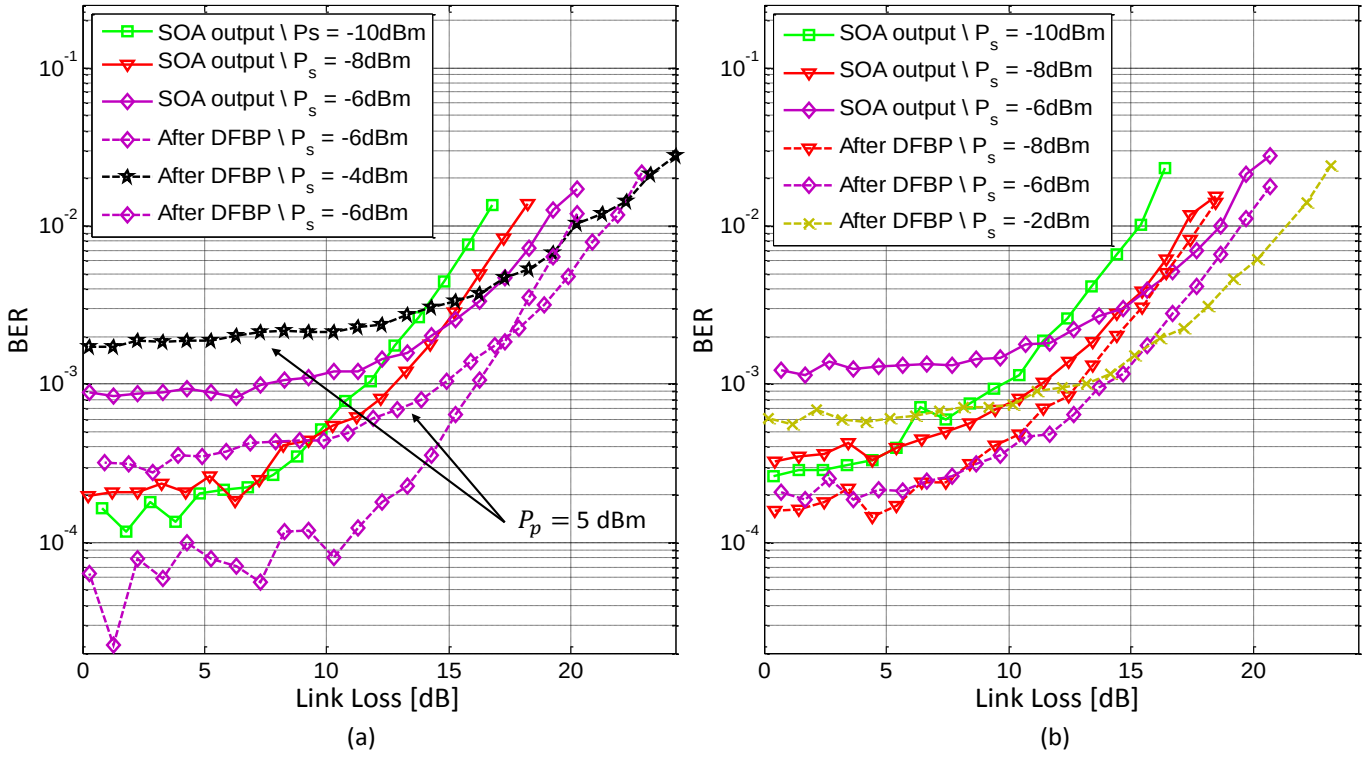

Fig. 12 Measured BER as a function of the link loss of 5 Gbaud 64QAM single stage wavelength conversion with (a) 35 dB input OSNR and (b) 25dB input OSNR.

achievable after DFBP with 25 dB input OSNR (see Fig. 12(b)). For instance, we obtain 2.7 dB link loss gain for a BER of 2×10^{-3}.

V. Dual Stage Wavelength Conversion

In this section we investigated the performance of a cascade of SOA WCs and examined the applicability of DFBP in this scenario. More specifically, we performed dual stage wavelength conversion of 5 Gbaud 64-QAM with 35 dB input OSNR. In these experiments, the two WC stages have the same operating conditions, i.e., input pump and signal power. To have the same signal power as the first WC stage input at the second WC stage input, the output of the first stage WC is amplified by an EDFA (EDFA5 in Fig. 1(b)) in order to compensate for the negative CE and the insertion losses of the optical filter (OF4 in (b)) and the 2×1 optical coupler used for the coupling with the pump. The signal at the second stage SOA input (SOA2 in Fig. 1(b)) shows a degraded $OSNR_{in}$ not only because of the noise figure of the first WC, but also because of EDFA5. This configurations shows the importance for the post-compensation technique to compensate nonlinearities even in the presence of signals with degraded OSNR. In section III, we showed that the proposed DFBP technique still improves significantly the EVM and BER with 25 dB input OSNR (see Fig. 6).

Fig. 13 displays the experimental results for 5 Gbaud 64-QAM dual stage wavelength conversion with 35 dB input OSNR. Fig. 13(a) shows the optimal EVM, i.e., with the optimal input signal power, for pump power of $P_p = 5$ dBm and $P_p = 10$ dBm as a function of the link loss after the second WC. The EVM for all input signal power values is shown for the particular cases of 0 dB, 4 dB and 8 dB link loss in Fig. 13(b), Fig. 13(c) and Fig. 13(d) respectively. All graphs display the EVM obtained without and with the use of DFBP. In Fig. 13(a), the EVM improvement after DFBP ranges from 0.5% to 0.8% depending on the WC operating condition. The crossing point where the optimal pump power shifts from $P_p = 10$ dBm to $P_p = 5$ dBm is 7 dB, both before and after DFBP. For the single stage wavelength conversion experiments with 35 dB input OSNR (see Fig. 11(a)), the crossing point was much higher, occurring at 22 dB before DFBP and 14 dB after DFBP. Because of the accumulated ASE noise in the cascaded WCs configuration, optimizing the WCs operating condition for maximum CE, even at the expense of additional nonlinearities, is the better solution even for low link loss value. This further justifies the utilization of a post-compensation technique of the nonlinear distortions induced by the WCs such as the one presented here.

Fig. 14 shows the measured BER as a function of the link loss for several operating conditions with 35 dB input OSNR. As in the previous section (see Fig. 12), only the operating conditions leading to an optimal BER, without and with DFBP to compensate nonlinear distortions, are shown and unless stated otherwise, the pump power is always 10 dBm. For the dual stage wavelength conversion experiment, a BER below the hard-decision FEC threshold of 2×10^{-3} is achievable only

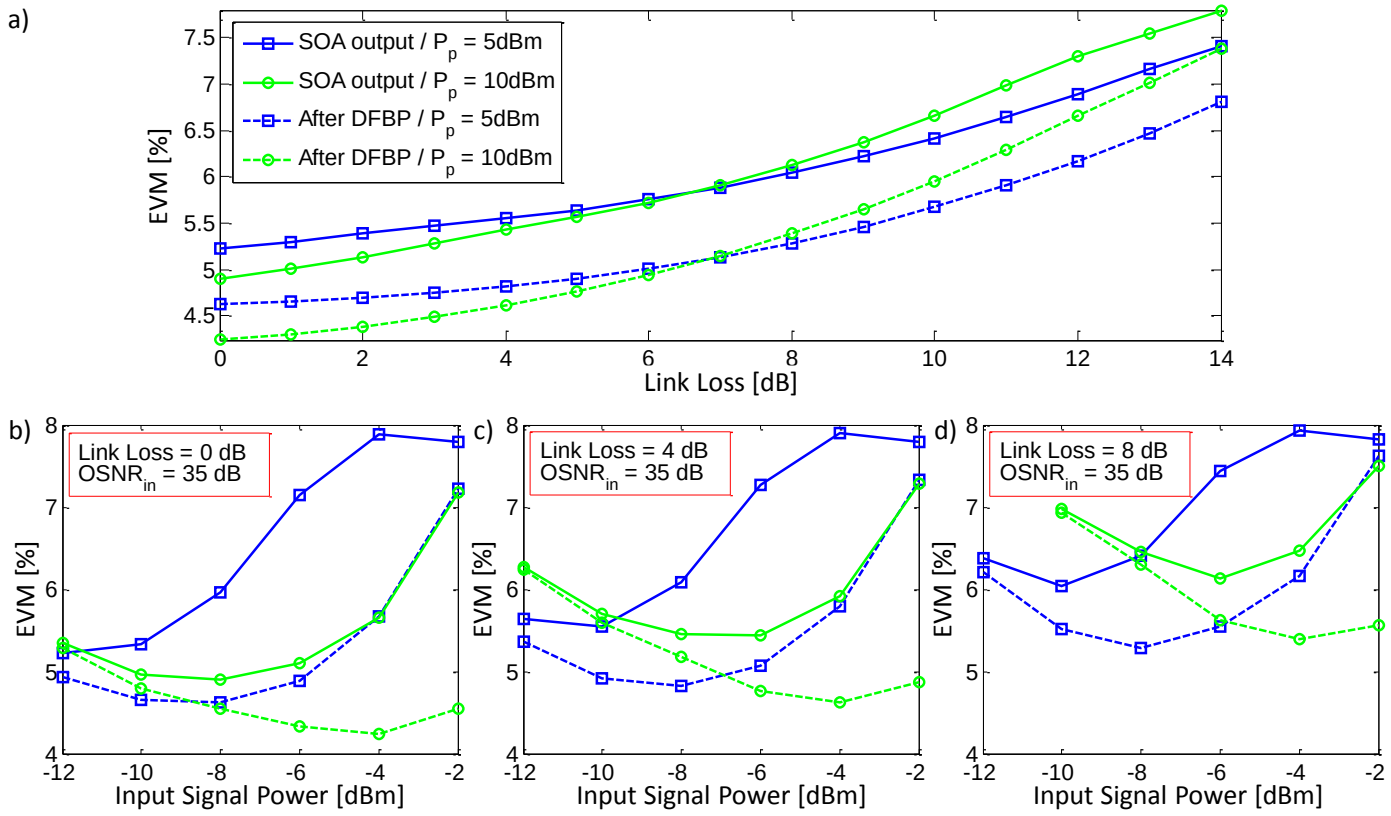

Fig. 13 a) Measured EVM with an optimal input signal power as a function of the link loss of 5 Gbaud 64QAM dual stage wavelength conversion. Measured EVM as a function of the input signal power for a link loss of a) 0 dB b) 4 dB and c) 8 dB. The EVM is shown before and after application of the DFBP post-compensation technique.

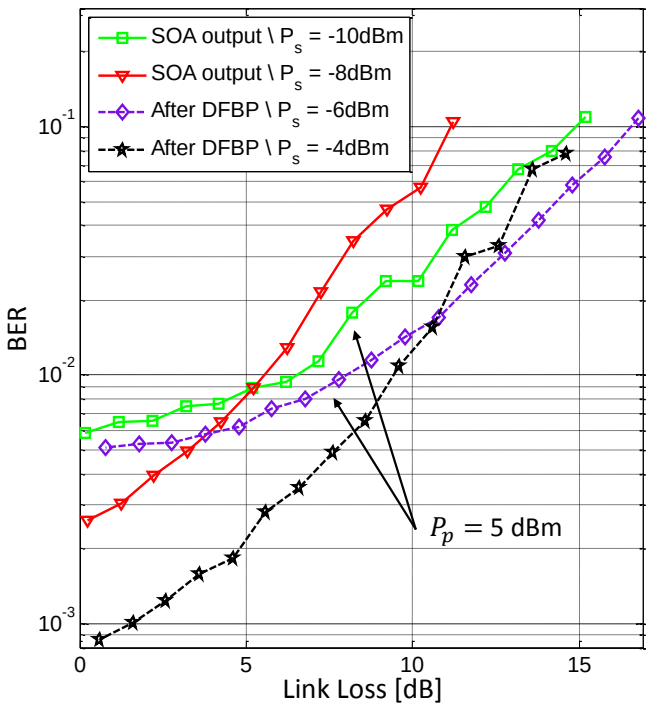

Fig. 14 Measured BER as a function of the link loss of 5 Gbaud 64-QAM dual stage wavelength conversion.

after DFBP up to 5 dB link loss indicating that the use of post-compensation technique is essential to obtain good system performance. However, a cascade of two wavelength conversion stages would be possible without post-compensation if we were to use a soft-decision FEC with a threshold of 2.4×10^{-2} [20]. Even in this context, performance is still significantly improved by the use of DFBP as shown by the 4.3 dB gain in the link loss budget.

VI. Conclusion

We experimentally investigated the performance of a novel low-complexity digital filter-based back-propagation technique to compensate the nonlinear distortions induced by a SOA-based WC when the input signal presents degraded OSNR. Our study specifically targets advanced modulation formats that are more susceptible to phase noise and, although we present representative results obtained with 64-QAM, we also demonstrated that the DFBP, while not presented here, is also effective with 16-QAM. We showed that this post-compensation technique improves the performance and reduces pump requirements of 5 Gbaud 64-QAM single stage wavelength conversion. We also investigated the operating condition of the WC and found that the optimal input pump power and signal power vary depending on the link following the WC. This optimization results from the tradeoff between the OSNR of the received signal and the nonlinearities induced by the WC. As the losses increase, it is preferable to optimize the pump power for maximum conversion efficiency, at the cost of additional nonlinear distortions of the wavelength converted signal. In this context, the use of the DFBP technique proves to be even more advantageous. Finally, we performed, for the first time to our knowledge, dual stage conversion wavelength 5 Gbaud 64-QAM. The experimental results show that a BER

; only achievable with
tortions. The reach and
ı a SOA for advanced
ıntly improved with the
s. Furthermore, the use
ıe number of possible
uted optical network.

RACTION

's of the SOA, i.e., the
e saturation power P_{sat}
in versus input power
and temperature were
ively. Fig. 15 illustrates
sus SOA input power.
the carrier lifetime τ_s
the EVM after DFBP
of section IV. The
Table I.

ameters

			Value (P_p = 10 dBm)
	gain		30 dB
α	Linewidth enhancement factor	1.5	1.5
P_{sat}	Saturation power	10 dBm	10 dBm
τ_s	Carrier lifetime	90 ps	130 ps

The effective carrier lifetime τ_s has a different value for $P_p = 5$ dBm and $P_p = 10$ dBm since it is function of the carrier density inside the SOA [21]. We note that a coarse estimation of the SOA parameters is sufficient to ensure good performance of the DFBP scheme.

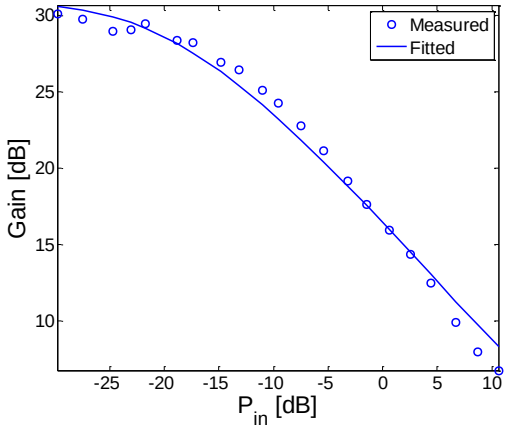

Fig. 15 Measured and least-squares fit of the static gain versus SOA input power.

References

[1] S. J. Ben Yoo, "Optical Packet and Burst Switching Technologies for the Future Photonic Internet," *J. Lightw. Technol.*, vol. 24, no. 12, pp. 4468–4492, Dec. 2006.

[2] L. Xu, W. Zhang, H. L. R. Lira, M. Lipson, and K. Bergman, "A hybrid optical packet and wavelength selective switching platform for high-performance data center networks," *Opt. Express*, vol. 19, no. 24, p. 24258, Nov. 2011.

[3] Q. Xu, H. Rastegarfar, Y. Ben M'Sallem, A. Leon-Garcia, S. LaRochelle, and L. A. Rusch, "Analysis of Large-Scale Multi-Stage All-Optical Packet Switching Routers," *J. Opt. Commun. Netw.*, vol. 4, no. 5, p. 412, Apr. 2012.

[4] C. Rottondi, M. Tornatore, and G. Gavioli, "Optical ring metro networks with flexible Grid and distance-adaptive optical coherent transceivers," *Bell Labs Tech. J.*, vol. 18, no. 3, pp. 95–110, Dec. 2013.

[5] P. Layec, A. Morea, F. Vacondio, O. Rival, and J.-C. Antona, "Elastic optical networks: The global evolution to software configurable optical networks," *Bell Labs Tech. J.*, vol. 18, no. 3, pp. 133–151, Dec. 2013.

[6] C. Tremblay, A. Enriquez-Castillo, M. P. Belanger, and F. Gagnon, "Filterless WDM optical core networks based on coherent systems," in *2011 13th International Conference on Transparent Optical Networks*, Jun. 2011, pp. 1–4.

[7] Q. Zhuge, M. Morsy-Osman, X. Xu, M. Chagnon, M. Qiu, and D. V. Plant, "Spectral Efficiency-Adaptive Optical Transmission Using Time Domain Hybrid QAM for Agile Optical Networks," *J. Lightw. Technol.*, vol. 31, no. 15, pp. 2621–2628, Aug. 2013.

[8] A. Mecozzi, S. Scotti, A. D'Ottavi, E. Iannone, and P. Spano, "Four-wave mixing in traveling-wave semiconductor amplifiers," *IEEE J. Quantum Electron.*, vol. 31, no. 4, pp. 689–699, Apr. 1995.

[9] B. Filion, W. C. Ng, A. T. Nguyen, L. A. Rusch, and S. Larochelle, "Wideband wavelength conversion of 16 Gbaud 16-QAM and 5 Gbaud 64-QAM signals in a semiconductor optical amplifier.," *Opt. Express*, vol. 21, no. 17, pp. 19825–33, Aug. 2013.

[10] B. Filion, A. Nguyen, L. Rusch, and S. LaRochelle, "Digital Post-Compensation of Nonlinear Distortions in Wavelength Conversion Based on Four-Wave-Mixing in a Semiconductor Optical Amplifier," J. Lightw. Technol., vol. 33, no. 15, pp. 3254–3264, May 2015.

[11] M. Shtaif and G. Eisenstein, "Analytical solution of wave mixing between short optical pulses in a semiconductor optical amplifier," *Appl. Phys. Lett.*, vol. 66, no. 12, p. 1458, May 1995.

[12] M. C. Jeruchim, P. Balaban, and K.Sam Shanmnugan, *Simulation of Communication Systems : Modeling, Methodology , and Thechniques*. 2002.

[13] M. Selmi, Y. Jaouen, and P. Ciblat, "Accurate digital frequency offset estimator for coherent PolMux QAM transmission systems," in *Optical Communication, 2009. ECOC '09. 35th European Conference on*, Sep. 2009, pp. 1–2.

[14] J. G. Proakis and D. K. Manolakis, *Digital Signal Processing: Principles, Algorithms and Applications (3rd Edition)*. Prentice Hall, 1995.

[15] S. Zhang, C. Yu, P. Y. Kam, and J. Chen, "Parallel Implementation of Decision-Aided Maximum-Likelihood Phase Estimation in Coherent M -ary Phase-Shift Keying Systems," *IEEE Photonics Technol. Lett.*, vol. 21, no. 19, pp. 1471–1473, Oct. 2009.

[16] P. J. Winzer, A. H. Gnauck, C. R. Doerr, M. Magarini, and L. L. Buhl, "Spectrally Efficient Long-Haul Optical Networking Using 112-Gb/s Polarization-Multiplexed 16-QAM," *J. Lightw. Technol.*, vol. 28, no. 4, pp. 547–556, Feb. 2010.

[17] B. Filion, W. C. Ng, A. T. Nguyen, L. A. Rusch, and S. Larochelle, "Wideband wavelength conversion of 16 Gbaud 16-QAM and 5 Gbaud 64-QAM signals in a semiconductor optical amplifier.," *Opt. Express*, vol. 21, no. 17, pp. 19825–33, Aug. 2013.

[18] G. P. Agrawal, *Fiber-Optic Communication Systems*, 3rd ed. New York, 2002.

[19] S. J. Ben Yoo, "Energy Efficiency in the Future Internet: The Role of Optical Packet Switching and Optical-Label Switching," *IEEE J. Sel. Top. Quantum Electron.*, vol. 17, no. 2, pp. 406–418, Mar. 2011.

[20] W.-R. Peng, T. Tsuritani, and I. Morita, "Transmission of High-Baud PDM-64QAM Signals," *J. Lightw. Technol.*, vol. 31, no. 13, pp. 2146–2162, Jul. 2013.

[21] M. J. Connelly, "Wideband semiconductor optical amplifier steady-state numerical model," *IEEE J. Quantum Electron.*, vol. 37, no. 3, pp. 439–447, Mar. 2001.

Benoît Filion was born in 1983. He received the B.S. degree in 2009 and M.S. degree in 2011 in electrical engineering from Université Laval in Canada. He is currently pursuing the Ph.D. in electrical engineering at Université Laval.

An T. Nguyen was born in 1982. He received the B.S. degree in physics in 2003 and M.S. degree in electronics engineering in 2007 from University of Science – Vietnam National University (VNU) in Ho Chi Minh City, Vietnam.

From 2008 to 2011, he was pursuing his Ph.D. degree in optical telecommunications at the Centro di Eccellenza per l'Ingegneria dell'Informazione, della Comunicazione e della Percezione (CEIICP) of Scuola Superioré Sant'Anna, Pisa, Italy. His research topics involved ultra-fast (640Gbps and beyond) OTDM subsystems, multifunctional hybrid add/drop node for OTDM and WDM integration, all-optical wavelength and modulation format converter, ultrafast packet switching and photonic digital processing circuits. From 2012 to 2015, he was a post-doc at the Centre d'Optique, Photonique et Laser (COPL), Université Laval, Québec, Canada. His projects focus on optical coherent detection systems with higher-order modulation formats, OFDM-over-fiber and full-duplex wireless-fiber interfacing. He is currently with Infinera Corp., California, United States, as a test developing engineer for new generations of photonic integrated circuit employed in coherent long-haul and metro communication systems.

Leslie Ann Rusch (S'91-M'94-SM'00-F'10) received the B.S.E.E. degree (with honors) from the California Institute of Technology, Pasadena, in 1980 and the M.A. and Ph.D. degrees in electrical engineering from Princeton University, Princeton, NJ, in 1992 and 1994, respectively.

Dr. Rusch has experience in defense, industrial and academic communications research. She was a communications project engineer for the Department of Defense from 1980-1990. While on leave from Université Laval, she spent two years (2001-2002) at Intel Corporation creating and managing a group researching new wireless technologies. She is currently a Professor in the Department of Electrical and Computer Engineering at Université Laval, QC, Canada, performing research on wireless and optical communications. She is a member of the Centre for Optics, Photonics, and Lasers (COPL) at Université Laval. Prof. Rusch's research interests include digital signal processing for coherent detection in optical communications, spatial multiplexing using orbital angular momentum modes in fiber, radio over fiber and OFDM for passive optical networks; and in wireless communications, optimization of the optical/wireless interface in emerging cloud based computing networks, optical pulse shaping for high-bit rate ultrawide-band (UWB) systems, and implantable medical sensors with high bit rate UWB telemetry.

Dr. Rusch is recipient of the IEEE Canada J. M. Ham Award for Graduate Supervision. Prof. Rusch has published over 100 journal articles in international journals (90\% IEEE/IEE) with wide readership, and contributed to over 140 conferences. Her articles have been cited over 3800 times per Google Scholar.

Sophie LaRochelle (M'00) received a Bachelor's degree in engineering physics from Université Laval, Canada, in 1987; and a Ph.D. degree in optics from the University of Arizona, USA, in 1992.

From 1992 to 1996, she was a Research Scientist at the Defense Research and Development Canada - Valcartier, where she worked on electro-optical systems. She is now a professor at the Department of Electrical and Computer Engineering, Université Laval, where she holds a Canada Research Chair (Tier 1) in Advanced Photonics Technologies for Communications. Her current research activities are focused on active and passive components for optical communication systems including silicon photonic devices, Bragg gratings filters, multi-wavelength and pulsed fiber lasers. Other research interests include optical fibers and amplifiers for spatial division multiplexing, all-optical signal processing and routing, and transmission of radio-over-fiber signals including UWB and GPS.

Dr. LaRochelle is an IEEE senior member and an OSA Fellow.